. Journal of Applied Mechanics and Technical Physics, Vol. 36, No. 1, 1995

TRANSFORMATION OF A DENSITY FIELD BY A THREE-DIMENSIONAL BODY MOVING IN A CONTINUOUSLY STRATIFIED FLUID

Yu. D. Chashechkin, E. V. Gumennik, and E. Ya. Sysoeva

UDC 532.5:681.7

Introduction. Perturbations introduced into a stratified fluid by the movement of the fluid past barriers of different types have been intensively studied under natural conditions [1] by mathematical [2] and physical [3] methods of modeling. The results obtained thus far are in fairly good agreement as regards the structure of large-scale phenomena — particularly associated (lee) waves [4]. However, the qualitative agreement between the theoretical representations and the measurements is clearly inadequate. One possible reason for the difference between theory and experiment might be that the assumption that the body has little effect on the structure of stratification near it is incorrect (in calculations, it is customary to assign the buoyancy frequency distribution in the depth direction).

A series of experimental studies showed that relatively thin high-gradient interlayers are formed at the boundaries of the wake in laminar flow about two-dimensional [5] and three-dimensional [6] bodies. In physical terms, the accompanying increase in the density gradient and the branching of the scales of three-dimensional changes in different physical fields are associated with the effects of molecular phenomena and the so-called dispersion of the medium (the difference in the coefficient of molecular diffusion of salt and the moment coefficient) on the spatial structure and stability of flows of a continuously stratified fluid. These effects are also seen in the simplest type of boundary-layer flow, induced by diffusion in a quiescent [7] or slowly moving continuously stratified medium [8], and they may persist far from the boundary with the separation of branched dynamic and density boundary layers from the body.

Experimental investigations of the evolution of density fields in stratified media should be performed using methods characterized by a high degree of sensitivity, good spatial resolution, speed, and a broad dynamic range. A contactless optical method was employed in [9] to obtain density gradient profiles in real time, the method having been based on the real-time recording of instantaneous values of the angle of refraction of a narrow probe beam from a laser that scanned the object. This method did not disturb the object in any way, and the time resolution (the minimum time between two profiles) was limited by the characteristics of the measurement system rather than by the physical properties of the object — as is the case when contact sensors are used [10]. Resolution could have been reduced to a value substantially below 10^{-2} sec in the method used in [9].

Our goal here is to quantitatively study the distortion and evolution of the density field in the uniform motion of a three-dimensional body in a continuosly stratified fluid. We will do this by synchronously recording shadowgraphs of the wake and the corresponding signals generated by a laser scanning refractometer.

Measurement Method. The studies [9, 11, 12] discussed methods that can be used to employ a laser scanning refractometer (LSR) in conjunction with a shadow instrument (SI). The authors of these investigations also analyzed the characteristics of the complementary optical system used for measurement. It was noted in [9] that combining the use of an LSR and a shadow instrument has several advantages and makes use of the distinctive features of each unit. First of all, the real-time quantitative data recorded by the LSR is obtained from the most informative regions of the test object — regions chosen on the basis of the results of preliminary visual analysis of the object's shadowgraph. Secondly, the reliability of the information obtained with the LSR is checked by visual observation of the shadowgraph. Thirdly, the quantitative analysis of shadowgraph obtained using such a system is simplified considerably, since the system automatically obtains necessary (for the analysis) data on the connection between the angles of deflection of the light rays and the corresponding levels of darkening on the shadowgraph. This makes it unnecessary to employ the standards of phase inhomogeneity that are normally used.

Moscow. Translated from Prikladnaya Mekhanika i Tekhnicheskaya Fizika, No. 1, pp. 20-32, January-February, 1995. Original article submitted April 30, 1994.

0021-8944/95/3601-0019$12.50

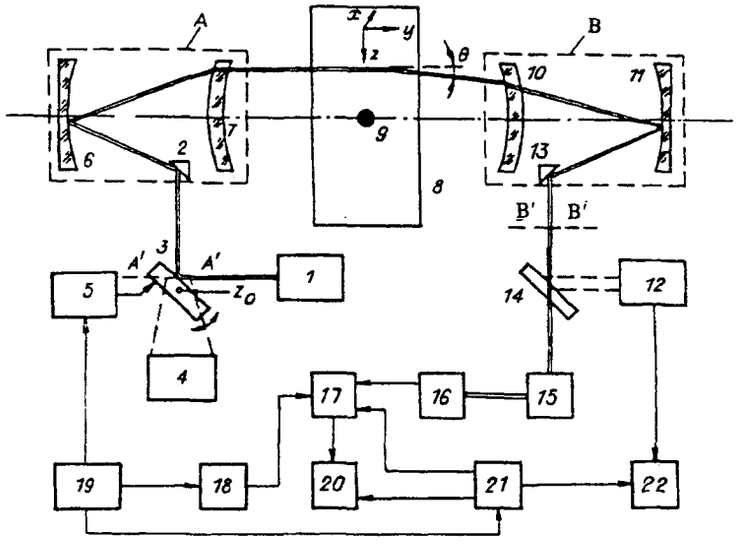

Fig. 1

In our experiments, the field of the density gradient was visualized by shadow methods with different orientations of the knife-edge and slit. These methods were realized on the basis of interference-shadow instrument IAB-458. Profiles of the vertical component of the density gradient were measured using an IAB-458 together with a laser scanning refractometer. The physical parameter measured in this case was the angle of refraction θ, which was determined by the gradient of the refractive index n integrated over the length of the probe beam (as in shadow methods)

$$\theta = \frac{1}{n_0} \int_0^L \frac{\partial n}{\partial z} dy$$

(n_0 is the refractive index of the medium surrounding the object) and the density gradient ρ. The latter is connected with the angle of refraction by the equation of state. This relationship is as follows for an aqueous solution of sodium chloride within the range of parameters that is of interest for the hydrodynamics of stratified flows [13]

$$\theta = \frac{0.231}{n_0} \int_0^L \frac{\partial \rho}{\partial z} dy, \text{ where } [\rho] = \text{g/cm}^3$$

We used a complementary optical system which combined a standard IAB-458 shadow instrument with a laser scanning refractometer. Figure 1 shows a diagram of this measurement system. The illuminating part of the serial IAB-458 instrument consists of the block 4 that forms the light beam, a diagonal mirror 2, and a collimating objective A formed by spherical mirror 6 and meniscus 7. Block 4 reflects the inlet slit of the IAB-458 onto focal plane A′ − A′ of lens A, resulting in the formation of a broad parallel light beam that probes the object 8.

The illuminating part of the LSR consists of the block 1 that generates and optimizes the parameters of the laser beam, scanner 3 (whose axis of rotation lies in the focal plane A′ — A′), diagonal mirror 2, and collimating objective A.

We were able to superpose the illuminating parts of the LSR and SI because the scanner mirror had a transmission factor of 50% and because the scanner was compact enough so that it could be installed inside the block 4 that forms the light beam. Such a method of combining the illuminating parts of the LSR and SI is considerably simpler than the scheme employed in [9]. Also, since the system does not require the use of additional tilting mirrors to align the objective (and since accompanying aberrations are thus not a problem), the given arrangement maximizes the accuracy of the LSR. The system employs a new type of scanner, the main elements of which are a stator and a rotor. The stator is composed of two current windings with a magnetic core and two permanent magnets. The rotor consists of a core made of a ferromagnetic alloy mounted on two bearings. One end of the rotor is attached to the mirror, while the other end is positioned coaxially with a torsion bar. In the scanning process, the mirror undergoes periodic vibrations as a result of a force moment acting on the core in a magnetic

field excited by current generated in the control winding. The current is generated in accordance with a periodic law established by means of scanner control block 5.

With the use of a 10 × 10 mm glass substrate 1 mm thick for the mirror of the scanner, the amplitude–frequency characteristic of the unit was such as to allow scanning at frequencies up to 100 Hz. This is quite adequate for the problems of the hydrodynamics of stratified flows that are of interest. The use of a scanner with a deflecting mirror of this size also allowed us to obtain a laser beam of sufficiently large cross section ($\sim 10/\sqrt{2}$ mm) in the focal plane of objective A. In accordance with the results reported in [9], the use of a relatively large beam in turn made it possible to significantly improve the spatial resolution of the LSR compared to the alignment system employed previously. Thus, the method devised here to combine the illuminating parts of the LSR and shadow instrument allowed us to develop a measurement system with superior accuracy and spatial resolution.

The broad probe beam formed by objective A passes through the test object and, assuming that the optical system is properly adjusted [13], strikes the receiving objective B. This objective is composed of the meniscus 10 and spherical mirror 11. With the aid of diagonal mirror 13 and half-silvered mirror 14, the beam is then directed to the block 12 that forms the shadowgraph. The shadowgraph is recorded by RFK-5 motion picture camera 22. Block 12 employs various types of visualizing diaphragms — Foucault knife-edge, filament, grating (for color shadowgraphs).

The receiving part of the LSR consists of the receiving objective B, mirror 13, half-silvered mirror 14, optics matching block 15, and coordinate-sensing photodetector (CSP) 16.

The receiving parts of the LSR and SI are aligned by means of the half-silvered mirror and matching block, which optically matches the focal plane B′ — B′ of the objective B and the photosensitive surface of the CSP. A detailed description of the operation of the receiving part of the SI and linked LSR was presented in [9].

As the test object is scanned by the laser beam along the z axis, the amplitude of the electric signal u(t) at the output of the CSP is such that the scan time is less than the characteristic time of density variation in the object. Signal amplitude is determined from the relation [12]

$$u(t) = Bf(0{,}231/n_0)R(z), \tag{1}$$

where B is the curvature of the coordinate characteristic of the CSP; f is the focal length of the receiving objective of the LSR;

$$R(z) = \int_0^L (\partial\rho/\partial z)dy;$$

L is the size of basin 8 in the y direction.

For the scheme described above to combine the operation of an LSR and SI, Eq. (1) is transformed as follows with allowance for the optical properties of the optics matching block:

$$u(t) = BV_t f(0{,}231/n_0)R(z) \tag{2}$$

(V_t is the magnification of block 15 in the transverse direction).

Strictly speaking, Eq. (2) relates only the absolute values of u(t) and R(z) to one another, since the signal of the coordinate-sensing photodetector — designed on the principle of a differential amplifier — may be altered by the instrument settings for the same given direction of displacement of the cross section of the laser beam on the photosensitive surface of the CSP. However, in order to be able to correctly analyze experimental results, it is necessary to make allowance for the signs of R(z) and u(t) in this relation, in accordance with the orientation of the axes of the chosen laboratory coordinate system. We checked for agreement between the signs empirically by slowly moving a standard long-focus lens vertically in the system lens space while the position of the probe beam (from the laser) was fixed. Equation (2) was then corrected to account for the relationship of the signs so that u(t) decreased if the density gradient in the region of the object probed by the laser beam increased above the background level (taken as zero). Conversely, a decrease in the density gradient led to an increase in the output voltage.

Signal (2) from the output of the CSP entered the signal input of oscillograph 17. The input of the oscillograph that controls scanning simultaneously received a signal generated by the scanning-control unit of oscillograph 18. The operation of scanner control block 5 and the scanning-control block of oscillograph 18 were synchronized by master oscillator 19, which

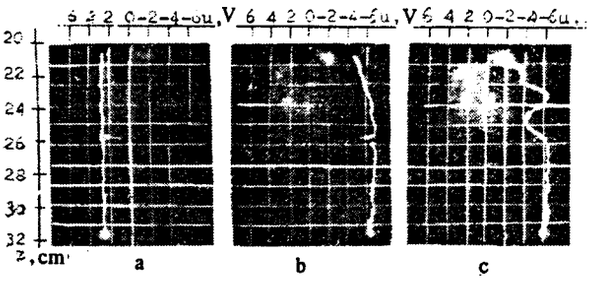

Fig. 2

also established the laws for scanning by the probe beam along the z axis in the laboratory coordinate system and horizontal scanning of the oscillograph along the t axis. Here, the vertical coordinate z in the physical space of the object was shown along the t axis of the oscillograph in the appropriate scale (determined by the scanning-control block), while the value of R(z) was shown along the other axis in accordance with law (2), i.e., the screen of oscillograph 17 "outlined" the vertical profile of the parameter R(z), characterizing the field properties of the density gradient in the object. The LSR signal, depicted in the same manner as just described on the screen of oscillograph 17, was recorded by RFK-5 motion picture camera 20.

The metrological characteristics of the LSR were analyzed in [9]. Here, we give numerical values of the main specifications only: sensitivity $5 \cdot 10^3$ V/rad; dynamic range 10^{-5}-10^{-3} rad; length of scanning line 110 mm; time constant no greater than $5 \cdot 10^{-6}$ sec; time resolution 0.5 mm.

Figure 2 presents examples of LSR signals obtained under different conditions: a) in a homogeneous medium [here, the central peak of the signal with the double maximum is connected with the diffraction of the scanning beam (from the laser) on the filaments of the towing device]; b) in an appreciably stratified medium before the beginning of towing of a sphere. The shallow slope of the overall curve can be attributed to the fact that the actual distribution law of density along the vertical coordinate z deviates from linearity when the basin is filled. Estimates show that these deviations lie within the range 5-10% when the LSR is used to monitor filling of the basin with a stratified liquid by the continuous displacement method (Fig. 2c).

An important element of the measurement system being described here is the ability to compare information recorded in two different channels — by means of the shadow instrument and the LSR. Such compatibility was achieved through the use of a unit that synchronizes the operation of motion picture cameras 20 and 22. The operation of this device is in turn controlled by the master oscillator, which synchronizes the operation of the measurement system as a whole. The unit 21 is a commutation switch that controls the supply of power to the recording cameras.

The thresholds for activation of the corresponding electronic switches are set independently of one another and are related to the electric signal that controls the operation of the scanner and the outer sweep of the oscillograph. The experimenter watches the oscillograph screen for the moments when the camera is tripped in relation to the position of the scanning beam in the laboratory coordinate system. These moments are selected by adjusting the block to conform to the conditions of the experiment. Thus, shadowgraphs providing information on the behavior of the test object as a whole (diameter of the field 230 mm) are correlated with LSR signals providing quantitative information on the vertical profile of the density gradient (characteristic dimension of the beam in the region of the object ~ 0.5 mm, size of the scanning line 110 mm).

The experiments were conducted in a rectangular basin measuring 0.7 × 0.25 × 0.7 m. The basin was filled with a stratified solution of sodium chloride. The distribution of density in the depth direction was linear. The buoyancy period of the stratified medium was checked with a density marker behind a surfacing gas bubble [15] and was determined to be T_b = 12 and 4.5 sec. A sphere of the diameter d = 4 cm was moved at a constant velocity U along a stationary guide wire 0.5 mm in diameter. The wire passed through the center of the sphere. The lead wire (0.15-mm constantin wire) was positioned parallel to the guide wire 1 mm from it. Such a towing system made the motion of the sphere as uniform as possible and eliminated vibrations and sticking. We also saw no evidence of turbulence ahead of the body. Turbulence could have been produced by the interaction of the flow in the developing boundary layer and the moving guide wire passing through the center of the body [16]. The interval between separate tests was 3-4 h. The original profile of the density gradient was reestablished during this time — a process monitored by the LSR.

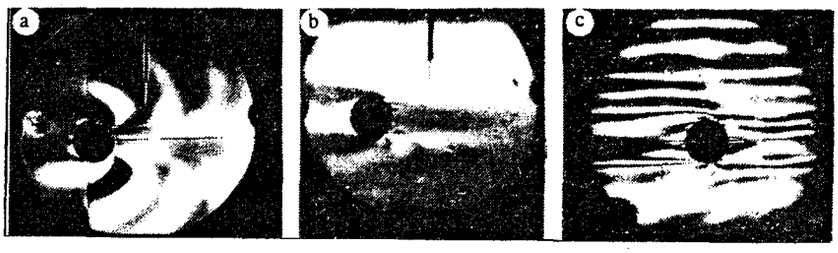

Fig. 3

Results. An analysis of numerous flow-visualization experiments conducted within a broad range of Reynolds and Froude numbers ($7 < Re = Ud/\nu < 2000$, $10^{-4} < Fr = U^2/N^2d^2 < 10^2$, where ν is kinematic viscosity and $N = 2\pi/T_b$ is buoyancy frequency) allowed us to construct the overall wake pattern created behind the body in the stratified medium. We were thus able to discern the following structural elements: obstructed fluid ahead of the body, associated internal waves, dynamic (velocity) and density boundary layers on the surface of the body, a wake behind the body — including dynamic and density wakes [5, 6]. The experiments thus revealed two new structural elements, i.e., the density boundary layer on the body and the density wake. The latter was bounded by high-gradient envelopes of fluid that were clearly visible in the shadow visualization. These elements correspond to the following scales [5]: the dynamic scale $\delta_\nu = \nu/U$, characterizing the thickness of the velocity (dynamic) boundary layer; the density scale $\delta_s = k_s/U$ (k_s is the diffusion coefficient of salt), characterizing the thickness of the density boundary layer. The substantial difference seen in the values for the buoyancy scale $\Lambda = (d\ln\rho/dz)^{-1}$ ($N = 2\pi/T_b = \sqrt{g/\Lambda}$) and the scales δ_ν and δ_s — a consequence of the difference in the kinetic coefficients (Schmidt number $Sc = \nu/k_s = 700$) — is a manifestation of a difference in the thicknesses of typical structural elements (splitting of the density and velocity boundary layers) and the thicknesses of the velocity-displacement layer δ_U and density-displacement layer δ_ρ at the boundary between the wake and the external field of internal waves. In the case of salt stratification, the ratio of the scales of variation of velocity and density at the boundary of the wake $\delta_U/\delta_\rho = 20 \sim \sqrt{Sc}$ for the motion of a sphere. This result is consistent with calculations of boundary-layer thicknesss performed in [7, 8].

Figure 3 shows photographs of laminar flow behind the sphere. The photographs were obtained by different shadow methods: a) vertical slit — Foucault knife-edge; b) slit — knife-edge, inclined at a 45° angle; c) black-and-white replica of a colored shadowgraph obtained with a horizontal grating [17].

The highest-constrast elements in Fig. 3a, showing the results of visualization of the horizontal component of the density gradient, are the associated internal waves — diffuse light and dark semicircles filling the entire field of the shadowgraph; the high-gradient envelopes around the density wake are visualized in the form of two thin horizontal bands recorded at a distance on the order of the diameter of the body; the associated internal waves do not penetrate the density wake.

The use of a technique which entails inclination of the knife-edge and slit turns out to be more convenient for visualizing density layers. If the slit and knife-edge are positioned at 45° to the horizon, then the vertical and horizontal components of perturbations of the density gradient will contribute equally to the shadowgraph. Almost no internal waves are seen in this case, but the separation of high-gradient layers from the body is readily visible. These layers were recorded over the entire length of the field of vision (Fig. 3b). The comparative analysis made in Fig. 3, a and b, shows that the density wake, bounded by high-gradient interlayers, has a density gradient with a complex internal structure.

Color shadowgraphs permit visualization of the vertical component of the density gradient. A region of obstructed fluid between closed isopleths ahead of the body can be seen in the black-and-white replica of a color shadowgraph we obtained (Fig. 3c). The curvature of the isopleths and the fine structure of the shadowgraph near the poles of the sphere indicate that there has been an increase in the initial density gradient and that a density boundary layer has formed.

In one case, measurements were made of the angles of separation of the density wake by using shadowgraphs obtained with different orientations of the slit and knife-edge [18]. These measurements showed that the position of the points of separation of the density boundaries of the wake are independent of the method used to visualize the flow.

In the experiments in which the LSR and SI were used simultaneously, we employed a method in which the knife-edge and slit were positioned vertically to permit visualization of the horizontal component of the density gradient $\partial\rho/\partial x$, when no dispersion of the medium is seen. In this case, the LSR signal was proportional to its vertical component $\partial\rho/\partial z$. Figure 4 shows

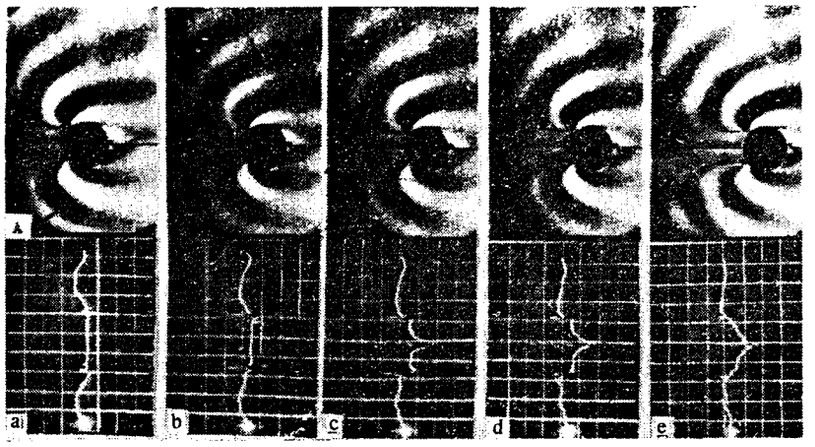

Fig. 4

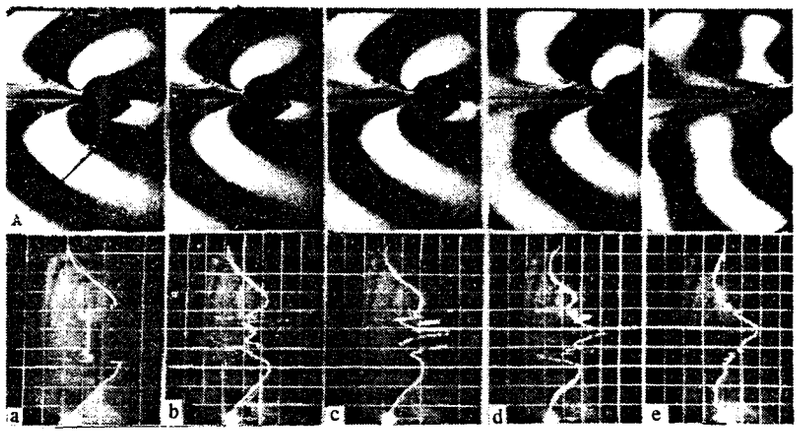

Fig. 5

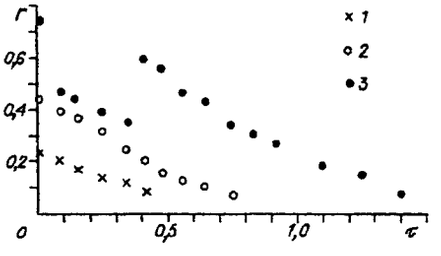

Fig. 6

a sequence of shadowgraphs of the wake and the corresponding sequence of LSR signals with the motion of a sphere d = 4 cm at the velocity U = 0.32 cm/sec in a fluid with a buoyancy period T_b = 12 sec (Re = 128, Fr = 0.09, C = Λ/d = 897). Scanning was done at a frequency of 1 Hz. The interval between frames was 2 sec. Internal waves and high-gradient envelopes around the density wake were visualized on the shadowgraphs, while marker A (the lowest position of the laser beam) indicates the position of the section in which the scanning was done. The first frame (Fig. 4a) of the LSR signal in the sphere corresponds to the horizontal diameter of the sphere, while the vertical section of the signal is due to the shielding of the laser

TABLE 1

Fr	Re	T_v = 4.5 sec, $\rho_0' = \left[\frac{\partial\rho}{\partial z}\right]_b$ = $2\cdot10^{-3}$ g/cm^4		T_v = 12 sec, $\rho_0' = \left[\frac{\partial\rho}{\partial z}\right]_b$ = $3\cdot10^{-4}$ g/cm^4	
		$\rho' = \frac{\partial\rho}{\partial z}$, g/cm^4	$\Gamma = \rho'/\rho_0$	$\rho' = \frac{\partial\rho}{\partial z}$, g/cm^4	$\Gamma = \rho'/\rho_0$
0,07	104	$0{,}72\cdot10^{-4}$	0,24	$2{,}4\cdot10^{-4}$	0,12
0,09	128	$1{,}2\cdot10^{-4}$	0,4	$2{,}4\cdot10^{-4}$	0,12
0,12	240	$2{,}2\cdot10^{-4}$	0,74	$2{,}6\cdot10^{-4}$	0,13

TABLE 2

Fr	Re	T_v = 12 sec, ρ_0' = $[\partial\rho/\partial z]_b = 3\cdot10^{-4}$ g/cm^4		T_v = 4.5 sec, ρ_0' = $[\partial\rho/\partial z]_b = 2\cdot10^{-3}$ g/cm^4	
		$\rho' = \frac{\partial\rho}{\partial z}$, g/cm^4	$\Gamma = \rho'/\rho_0$	$\rho' = \frac{\partial\rho}{\partial z}$, g/cm^4	$\Gamma = \rho'/\rho_0$
0,07	104	$0{,}12\cdot10^{-4}$	0,04	$0{,}3\cdot10^{-4}$	0,015
0,09	128	$0{,}3\cdot10^{-4}$	0,1	$0{,}6\cdot10^{-4}$	0,03

TABLE 3

Fr	Re	T_v = 12 sec, $\rho_0' = 3\cdot10^{-4}$ g/cm^4	T_v = 4.5 sec, $\rho_0' = 2\cdot10^{-3}$ g/cm^4
		$\Delta\rho' = \rho'_{max} - \rho'_{min}$, g/cm^4	$\Delta\rho' = \rho'_{max} - \rho'_{min}$, g/cm^4
0.07	104	$0{,}6\cdot10^{-4}$	$1{,}2\cdot10^{-4}$
0,09	128	$0{,}7\cdot10^{-4}$	$2{,}1\cdot10^{-4}$
0,12	240	$1{,}2\cdot10^{-4}$	$2{,}5\cdot10^{-4}$

beam by the sphere. The perturbations of the signal at the beginning and end of the vertical section are connected both with diffraction effects at the edges of the sphere and with the increase in the density gradient in the density boundary layer on the sphere's surface.

The difference between the LSR signals and the background in the neighborhood of the sphere is connected with the distortion of the initial field of the density gradient by associated internal waves. In Fig. 4b, the scanning plane intersects the density envelope around the wake in the region of its separation from the sphere. It is then shielded by the sphere and again intersects the envelope. In the LSR record, the intersection of the envelope by the laser beam coincides with an abrupt change in the level of the signal connected with the increase in the density gradient at the boundaries of the wake. The signal is not shielded by the sphere when the next section is scanned (Fig. 4c). The beam passes through the wave region, intersects the density envelope (which produces peaks on the LSR record), passes through the internal region of the wake, intersects the second density envelope, and again enters the wave field. The disruption in the LSR signal at the center of the record is due to deflection of the laser beam on the guide and lead wires.

The density gradient becomes stronger throughout the internal region of the wake — the LSR signal decreases to a level 10% below the background (Fig. 4, c and d). In commonly used models, the density gradient decreases at the center of the wake due to partial mixing of the fluid [2]. We thus devoted our attention to the problem of establishing a correspondence between the sign of the LSR and the sign of the change in the density gradient. We attempted to do this by conducting special control measurements. The method used to obtain these measurements was described in the previous section. The vertical distribution of the density gradient inside the wake (Fig. 4, c and d) is characterized by the fact that a constant gradient is maintained on the periphery of the wake, while in the central part the gradient increases to a level more than 20% above the background:

$$\partial\rho/\partial z_v = \text{const}(z_v) \text{ at } d/6 < |z_v| < d/2$$

(Fig. 4c). Here, z_v is the vertical coordinate in the coordinate system connected with the center of the wake. A fine internal structure is formed in the density field inside the wake during the relative time $\tau = t/T_b = 0.5$, this structure being characterized by a linear change in the density gradient in the vertical direction (Fig. 4e). The discontinuities in the gradient at the boundaries of the wake become markedly smaller but remain present for the period $\tau = 3$.

Figure 5 shows the sequence of frames obtained with the motion of a sphere d = 4 cm with U = 0.6 cm/sec, T_b = 12 sec (Re = 240, Fr = 0.12, C = 897). In this regime, there is small-scale instability at the boundaries of the wake and an eddy is formed in its expansion region [6]. The point of separation of the density wake from the body is closer to the line of motion than in the previous case. Figure 5a corresponds to the scan made of a section passing through an opaque sphere. The density field is considerably more distorted in the region of this sphere than in Fig. 4a, the increase in distortion being due to associated internal waves.

Figure 5b presents the vertical profile of the density gradient corresponding to a section passing through the density envelopes of the wake in the region of their separation from the sphere. Figure 5c shows the same for a section passing through the "neck" of the wake. The vertical profile of the gradient in this case indicates that the wake has a relatively narrow (0.3d) central region characterized by a large increase in the gradient ($\Gamma = 0.5$, where $\Gamma = (\partial\rho/\partial z)/(\partial\rho/\partial z)_b$, $(\partial\rho/\partial z)_b$ being the density gradient of the background). Figure 5d corresponds to the intersection of the scanning beam and the wake in the region of the eddy. This vertical profile characterizes the sharp increase in the gradient in the region of the density envelopes around the eddy. After $\tau \sim 1.3$ (Fig. 5e), the gradient decreases substantially in the density layers at the boundaries of the wake and its internal structure is altered. In the new structure, the vertical profile of the gradient undergoes a smooth change in accordance with a law that is close to linear.

An important element of the density field behind a body moving in a stratified medium is the envelope of the wake. Within this envelope, abrupt changes in the density gradient take place over short distances in three directions. In our experiments, the largest changes recorded in the vertical component of the gradient in the density boundary layers were about 0.75 of the background gradient. According to our analysis of the LSR records, these layers had a thickness of approximately 0.8 mm. However, since the size of the probe beam in this region was 0.5 mm, we might have underestimated the changes in the gradient. The thickness of the boundary layers might have been overestimated as a result of spatial averaging.

Figure 6 shows time dependences of the relative change in the vertical component of the density gradient Γ in density envelopes of the wake. The results are shown for the following regimes: 1) Re = 104, Fr = 0.07; 2) Re = 128, Fr = 0.09; 3) Re = 240, Fr = 0.12 (d = 4 cm, T_b = 12 sec). Within the range of hydrodynamic parameters we studied, the density gradient at the boundaries of the wake increase with an increase in the Reynolds number. The increase in the gradient within the density layers is smaller in the laminar regime. Here, the gradient decreases to the background level after $\tau = 0.4$ for Re = 104 and $\tau = 0.8$ for Re = 128. The rate of decrease in Γ is also a function of time and changes at $\tau = 0.25$ for Re = 104 and $\tau = 0.5$ for Re = 128. The density gradient changes suddenly in the regime Re = 240, this change being connected with restructuring of the flow and an additional increase in the gradient in the density boundaries of eddies that are in the process of forming. Table 1 shows the maximum values of the density gradients at the boundaries of the wake.

A characteristic feature of the vertical profile of the density gradient in a laminar wake is an increase in the gradient inside the wake to a certain constant value. In the LSR records, this is manifest by the signal remaining constant as the inside of the wake is scanned (Fig. 4, b and c). Table 2 shows these constant values in the laminar regimes we studied.

The region in which the initial density gradient is distorted ahead of a body moving in a stratified fluid was classified in [19] as a region of obstructed fluid. In the case of the motion of a two-dimensional body, the obstruction is explained by the fact that the fluid particles around the body do not have enough kinetic energy to overcome the potential barrier associated with the initial stratification. The obstruction phenomenon is more complicated in the case of the motion of a three-dimensional body, since flow around the body in the horizontal plane is also then possible. However, in this case, shadowgraph visualization shows that perturbations exist ahead of the sphere (see Fig. 3).

We found in our experiments that the deformation of the profile of the vertical component of the density gradient ahead of the moving sphere is manifest as a reduction in the gradient relative to the background in the central part of the region and an increase in the gradient at the edges. The increase is the result of wave disturbances. The LSR record and the corresponding shadowgraph for the flow ahead of the sphere are shown in Fig. 7 (Re = 240, Fr = 0.12). Table 3 shows the maximum amplitudes of the vertical profile of the density gradient $\Delta\rho' = \rho'_{max} - \rho'_{min}$ for different regimes. These amplitudes increase

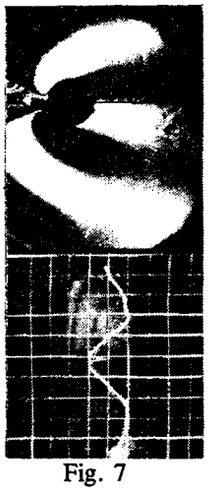

Fig. 7

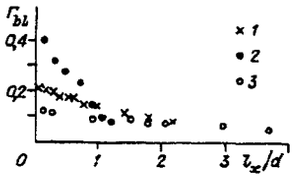

Fig. 8

with an increase in the Reynolds number (for fixed stratification) and a decrease in the Froude number (for an assigned velocity). Figure 8 shows the dependence of the gradient in the obstruction region Γ_{bl} on the relative distance l_x/d from the sphere [1) U = 0.32 cm/sec, T_b = 12 sec, Re = 128, Fr = 0.09; 2) U = 0.6 cm/sec, T_b = 12 sec, Re = 240, Fr = 0.12; 3) U = 0.6 cm/sec, T_b = 4.5 sec, Re = 128, Fr = 0.09]. We should point out that the differences in the hydrodynamic conditions had no effect on the vertical profiles of the density gradient ahead of the sphere even at the distance l_x/d = 1.5. The main changes took place at distances on the order of the diameter of the body. At l_x/d = 4, the profile of density ahead of the sphere was nearly the same as the background distribution.

Conclusion. Our tests show that the character of deformation of the density field due to the movement of a stratified fluid about obstacles has several distinctive elements. Specifically, there is a *decrease* in the initial gradient ahead of the body (within the region of obstructed fluid) and an *increase* in the gradient in the density wake behind the body. Thin high-gradient interlayers are formed at the periphery of the density wake. The character of distortion of the density profile is consistent with the flow scheme proposed in [19] and is independent of the particular details of the system set up to tow the body. The eddies observed to have formed in front of the body in [16] in the region of interaction of the boundary-layer flow and the lead wire were erroneously associated with an obstructed region by the authors of [20]. In the given series of experiments, the moving lead wire did not pass through the center of the body, no loss of stability was seen in the boundary-layer flow, and no eddies were formed.

An analysis of measurements made with an LSR and shadow instruments for all tests involving spheres [6, 16, 18, 19] shows that regardless of the Reynolds and Froude numbers, a region of fluid with a reduced density gradient is formed in front of the barrier. The existence of such a region is the clearest indication of obstruction of the flow.

Obstruction due to the combined effects of dissipation and buoyancy is manifest physically in the accumulation of fluid ahead of the body. Most of this fluid comes from the level at which the center of the body is moving. The degree to which the initial density profile is smoothed out and the length of the region in which gradient anomalies are seen ahead of the body (the height of this region being determined by the diameter of the obstacle, not by the length of the associated internal wave $\lambda = UT_b$) depend on the shape, dimensions, and velocity of the body and the degree of stratification. However, the fact that the gradient decreases ahead of the body is unquestioned, with a decrease in the gradient being consistently seen in all experiments involving the flow of either three-dimensional or two-dimensional obstacles (the details of the suspension system and the form of the body are immaterial).

The increase in the gradient in the wake of the body is connected with the same obstruction phenomenon. Here, the fluid displaced from the front of the body is replaced by fluid from overlying and underlying layers having their own densities. Depending on the parameters of motion, there may be one high-gradient wake [5, 21] or two relatively thin layers with an increased density gradient [6, 21]. Such a nonlocal pattern of deformation of the density field differs significantly from the model described in [2], where mixing behind the body caused the gradient to decrease at the center of the wake and increase on its periphery. In a system in which obstruction and displacement take place, the layer with the largest density gradient may be located at the center of the density wake of the body. The relatively smooth distortion of the density-gradient field is ac-

companied by the formation of very thin high-gradient interlayers. These layers are associated with separation of the density boundary layer from the body and the formation of a boundary between the fluid flowing around the body (which is initially in front of the body and then behind it) and the fluid in the wake (which, in the coordinate system of the body, consists of particles that are always behind the obstacle). The particles of the wake move toward the body along the axis of the wake — where the induced flow velocity is higher than the velocity of the body — and they move away from it along the wake's periphery.

Although the measurements indicate that the density gradient in such interlayers increases only slightly over the initial value, the effect of this increase is quite large. It is related to the change that occurs in the symmetry of the density wake, which is prismatic in form for a broad range of parameters [18, 22]. The interlayers also affect the stability of the flow and the structure of the eddies that are formed [5, 23].

Thus, our experimental results agree qualitatively with the flow scheme described in [19] and illustrate the need for more detailed investigation of the small-scale structure of wakes of stratified flows. The goal of such studies would be to accumulate quantitative data necessary for the development and testing of mathematical models.

The investigation described here was carried out with the financial support of the Russian Fund for Basic Research (Grant No. 93—05—8291, "Astrophysical and Geophysical Hydrodynamics").

REFERENCES

1. V. N. Kozhevnikov, "Orographic disturbances in a two-dimensional steady-state problem," Izv. Akad. Nauk SSSR Fiz. Atmos. Okeana, **4**, No. 1, 33-42 (1968).
2. Yu. M. Lytkin and G. G. Chernykh, "Flows that are similar with respect to the density Froude number and the energy balance in the evolution of turbulent mixing regions in a stratified medium," Din. Sploshnoi Sredy, **47**, 70-89 (1980).
3. V. I. Bukreev, A. V. Gusev, and I. V. Sturova, "Generation of internal waves in the simultaneous translation and vibration of a cylinder in a two-layer liquid," Prikl. Mekh. Tekh. Fiz., No. 3, 63-70 (1986).
4. P. Bonneton, J. M. Chomaz, and E. J. Hopfinger, "Internal waves produced by the turbulent wake of a sphere moving horizontally in a stratified fluid," J. Fluid Mech., **254**, 23-40 (1993).
5. I. V. Voeikov and Yu. D. Chashechkin, "Formation of discontinuities in the wake of a cylinder in a stratified flow," Izv. Russ. Akad. Nauk Mekh. Zhidk. Gaza, No. 1, 20-26 (1993).
6. E. Ya. Sysoeva and Yu. D. Chashechkin, "Eddy systems of the stratified wake of a sphere," Izv. Akad. Nauk SSSR Mekh. Zhidk. Gaza, No. 4, 82-90 (1991).
7. A. V. Kistovich and Yu. D. Chashechkin, "Structure of a transient boundary layer on an inclined plane in a continuously stratified medium," Dokl. Russ. Akad. Nauk, **325**, No. 4, 833-837 (1992).
8. V. G. Baidulov and Yu. D. Chashechkin, "Effect of diffusion on boundary-layer flows in a continuously stratified fluid," Izv. Russ. Akad. Nauk Fiz. Atmos. Okeana, **29**, No. 5, 666-672 (1993).
9. E. V. Gumennik and B. S. Rinkevichyus, "Use of the refraction of a scanning laser beam to study the structure of transparent discontinuities," Teplofiz. Vys. Temp., **25**, No. 6, 1191-1200 (1987).
10. A. V. Gvozdev, V. I. Neklyudov, and Yu. D. Chashechkin, "Comparative analysis of the dynamic characteristics of contact sensors in a continuously stratified fluid," Izmer. Tekh., No. 4, 33-35 (1990).
11. E. V. Gumennik, O. A. Evtikheva, B. S. Rinkevichyus, and Yu. D. Chashechkin, "Combined use of quantitative and qualitative refractometric methods," Inzh. Fiz. Zh., **50**, No. 4, 597-604 (1986).
12. E. V. Gumennik and Yu. D. Chashechkin, "Study of the structure of stratified flows by the method of laser scanning," Prikl. Mekh. Tekh. Fiz., No. 2, 177-182 (1990).
13. D. E. Mowbray, "The use of schlieren and shadowgraph techniques in the study of flow patterns in density stratified fluids," J. Fluid Mech., **27**, Pt. 4, 595-608 (1967).
14. G. Oster, "Density gradients," Sci. Am., No. 12, 70-74 (1965).
15. V. I. Nekrasov and Yu. D. Chashechkin, "Measurement of the velocity and period of vibration of a fluid by the method of surface markers," Metrologiya, No. 11, 36-41 (1974).
16. V. S. Belyaev, S. A. Makarov, and Yu. D. Chashechkin, "Associated internal waves," Preprint No. 214, IPM AN SSSR, Moscow (1983).

17. V. A. Popov and Yu. D. Chashechkin, "Color shadow method," Dokl. Akad. Nauk SSSR, **24**, No. 5, 1130-1133 (1981).
18. E. Ya. Sysoeva and Yu. D. Chashechkin, "Experimental study of the vortex structure of a stratified flow behind a sphere," Preprint No. 447, IPM AN SSSR, Moscow (1990).
19. Yu. D. Chashechkin, "Hydrodynamics of a sphere in a stratified fluid," Izv. Akad. Nauk SSSR Mekh. Zhidk. Gaza, No. 1, 3-9 (1989).
20. Q. Lin, W. R. Lindberg, D. L. Boyer, and H. J. S. Fernando, "Stratified flow past a sphere," J. Fluid Mech., **240**, 315-354 (1992).
21. Yu. D. Chashechkin and I. V. Voeikov, "Vortex systems behind a cylinder in a continuously stratified fluid," Izv. Russ. Akad. Nauk Fiz. Atmos. Okeana, **29**, No. 6, 821-830 (1993).
22. E. Ya. Sysoeva and Yu. D. Chashechkin, "Three-dimensional structure of the wake of a sphere in a stratified fluid," Prikl. Mekh. Tekh. Fiz., No. 5, 59-65 (1988).
23. Yu. D. Chashechkin, "Visualization and identification of vortex structures in stratified wakes," Eddy Structure Identification in Free Turbulent Shear Flows: IUTAM Symp., Poltiers, France, Oct. 1922. Kluwer, Dordrecht (1993), pp. 393-403.